Journal of Energy Chemistry 54 (2021) 111–117

Contents lists available at ScienceDirect

Journal of Energy Chemistry

journal homepage: www.elsevier.com/locate/jechem

http://www.journals.elsevier.com/journal-of-energy-chemistry/

Conversion of CO_2 and H_2 into propane over $InZrO_x$ and SSZ-13 composite catalyst

Zhaopeng Liu [a,b,c,1], Youming Ni [a,b,1], Tantan Sun [a,b,c], Wenliang Zhu [a,b,*], Zhongmin Liu [a,b,*]

[a] National Engineering Laboratory for Methanol to Olefins, Dalian Institute of Chemical Physics, Chinese Academy of Sciences, Dalian 116023, Liaoning, China
[b] Dalian National Laboratory for Clean Energy, Dalian 116023, Liaoning, China
[c] University of Chinese Academy of Sciences, Beijing 100049, China

ARTICLE INFO

Article history:
Received 19 January 2020
Revised 27 April 2020
Accepted 29 April 2020
Available online 30 May 2020

Keywords:
CO_2 hydrogenation
$InZrO_x$+ SSZ-13
Propane
Oxygen vacancies
Acid strength

ABSTRACT

Direct converting carbon dioxide into hydrocarbon fuels and value-added chemicals would offer a very attractive approach for efficient utilization of CO_2 as a carbon resource. Although, olefins, aromatics and gasoline have been successfully synthesized by CO_2 hydrogenation, highly selective conversion of CO_2 and H_2 into C_{2+} hydrocarbon is still challenging due to a high C–C coupling barrier and inhibiting the production of other long-chain hydrocarbons. Here, we report a composite catalyst made of $InZrO_x$ and SSZ-13 molecular sieve ($InZrO_x$ + SSZ-13), which exhibits 74.5% propane selectivity at 623 K. The 8-MR micropores and the higher strength of the acid for SSZ-13 benefit the formation of propane. Compared with pure InO_x and m-ZrO_2, the composite oxide $InZrO_x$ containing more oxygen vacancies, exhibits to be more readily reduced by H_2 and easier to adsorb and desorb CO_2 within the reaction temperature. All those could be beneficial to the activation and conversion of H_2 and CO_2. The catalytic performance of $InZrO_x$ + SSZ-13 in CO_2 hydrogenation provides a potential for production of propane.

1. Introduction

Hydrogenation of the greenhouse gas CO_2 into hydrocarbon fuels or chemicals can not only decrease its emission to atmosphere but also effectively utilize some fluctuating renewable energies (such as solar, tidal, wind and biomass) via transforming them to electricity and then to H_2 by decomposing water [1–4]. CO_2 hydrogenation to methane that is Sabatier reaction [5,6], has been highly selectively realized over metal-based heterogeneous catalysts. Synthesis of C_{2+} (more than two carbon atoms) hydrocarbons is generally dependent on Fischer-Tropsch synthesis method [7–10]. Since the hydrocarbon products follow the Anderson–Schulz–Flory (ASF) distribution rules [11], obtaining single C_{2+} hydrocarbon is very challenging.

In order to break through the ASF distribution, a novel concept of catalyst designing, which is called oxide-zeolite composite catalyst, has recently been proposed by Bao and Wang et al. [4,12–23]. Since then, by continuously exploring the composite catalysts, a lot of valuable hydrocarbons such as lower olefins [12,13,16,24–26], aromatics [17,27–32], and gasoline [15,33,34] have been selectively synthesized in syngas conversion or CO_2 hydrogenation. Furthermore, in syngas conversion, controlling the selectivity to single hydrocarbon product has also made great progress over composite catalysts. The catalytic sites within the 8-membered ring side pockets of mordenite (MOR) could control the hydrocarbon product to ethylene (73% among hydrocarbons) over $ZnCrO_x$/MOR catalyst [14]. Low molecular-diffusion resistance for the short straight channels [0 1 0] of H-ZSM-5 results in ~70% selectivity of tetramethylbenzene over $ZnCr_2O_4$/H-ZSM-5 catalyst [35]. The choice of special zeolite materials is of course important, but CO, which can form carbonyl (ketene or acetyl) intermediates, also plays a key role in highly selective formation of ethylene or tetramethylbenzene. However, because the concentration of CO during CO_2 hydrogenation is generally not high, the mechanism of generating single hydrocarbon in syngas conversion could not work in CO_2 hydrogenation. So far, there has been no report on the hydrogenation of CO_2 to a single C_{2+} hydrocarbon.

Here, we report a composite catalyst made by $InZrO_x$ oxide and SSZ-13 molecular sieve ($InZrO_x$ + SSZ-13), which exhibits 74.5% propane selectivity among all the products excluding CO in CO_2 hydrogenation. The topology and acidic property of SSZ-13 play a key role in the highly selective formation of propane.

* Corresponding authors at: National Engineering Laboratory for Methanol to Olefins, Dalian Institute of Chemical Physics, Chinese Academy of Sciences, Dalian 116023, Liaoning, China.
E-mail addresses: wlzhu@dicp.ac.cn (W. Zhu), liuzm@dicp.ac.cn (Z. Liu).
[1] These authors contributed equally to this work.

https://doi.org/10.1016/j.jechem.2020.04.069

2. Experimental

2.1. Catalyst preparation

Indium nitrate hydrate ($In(NO_3)_2 \cdot xH_2O$, 99.9% metal basis), copper nitrate trihydrate ($Cu(NO_3)_2 \cdot 3H_2O$, 99%), zinc nitrate hexahydrate ($Zn(NO_3)_2 \cdot 6H_2O$, 99%), aluminum nitrate nonahydrate ($Al(NO_3)_3 \cdot 9H_2O$, 99%), ammonium carbonate ($(NH_4)_2CO_3$, 30.0% NH_3 basis), ammonium hydroxide (25 wt% NH_3 in H_2O) and the precursors of monoclinic ZrO_2 (denoted as m-ZrO_2 in this work) support were commercial reagent. All chemicals were used directly without further process.

The In_2O_3 oxide (denoted as InO_x) was prepared by calcination of $In(NO_3)_2 \cdot 2H_2O$ at 300 °C for 2 h under static air condition. The $InZrO_x$ oxide catalyst with InO_x nominal weight percentage of 25 wt% was prepared by a typical deposition–precipitation method. Briefly, 4.0208 g $In(NO_3)_3 \cdot 2H_2O$ dissolved in 50 mL deionized water, followed by adding 5.0 g of m-ZrO_2 powder (particle size less than 180 mesh) under vigorous stirring for 1 h. The diluted ammonia solution (25 wt% $NH_3 \cdot H_2O$ diluted by deionized water 5 times) was added drop-wise to adjust the pH of suspension to 9–10. The suspension was digested for 3 h and then separated by centrifugation, washed by deionized water thoroughly, dried at 383 K for 12 h, and then calcined under static air at 573 K for 4 h. Finally, the obtained oxide catalyst was denoted as $InZrO_x$ in this work.

Molecular sieves mentioned in this work were all commercial products. The commercial SSZ-13-Na molecular sieve was converted into NH_4^+ form by exchanging 3 g SSZ-13-Na with 100 mL NH_4NO_3 aqueous solution (a series concentration of 0.01, 0.03, 0.1, 0.3, 1, 3 $mol \cdot L^{-1}$) at 353 K for 3 h, followed by filtration and washing with deionized water three times. After repeating the above mentioned process twice, the desired sample was dried at 383 K for 10 h, followed by calcination at 823 K for another 4 h in air to obtain a series of SSZ-13-*x* catalysts (where, the SSZ-13-3 catalyst was denoted as SSZ-13 in this work).

A composite catalyst named $InZrO_x$ + SSZ-13 contained $InZrO_x$ oxide and SSZ-13 by simply mechanical mixing of granules (0.4–0.8 mm) of two components. The granules in $InZrO_x$ + SSZ-13 were carried out by pressing under 40 MPa. Another physically mixed catalysts named OX + ZEO (InO_x + SSZ-13, $InZrO_x$ + SAPO-34, $InZrO_x$ + SAPO-18, $InZrO_x$ + MOR, $InZrO_x$ + Y, $InZrO_x$ + Beta, $InZrO_x$ + ZSM-5) were made with same procedure. The weight ratio of oxides and zeolites for the composite catalysts was 2:1. $CuZnAlO_x$ catalyst with ratio of Cu:Zn:Al = 5:4:1 was prepared by co-precipitation.

2.2. Catalyst performance test

Catalytic reaction experiments were performed in a fixed-bed stainless steel reactor (9 mm inner diameter). Before test, the composite catalyst InO_x + SSZ-13 was reduced at 573 K for 4 h with 20 mL/min H_2. All products were kept in gas phase and analyzed online by an Agilent 7890B GC equipped with a HP-PLOT/Q capillary column connected to FID detector and a TDX-1 column connected to TCD detector. Methane was used as a reference bridge between TCD and FID. Argon was used as an inner standard. Hydrocarbon distribution was based on carbon atoms number. CO_2 conversion, CO selectivity, and hydrocarbons (C_nH_m), methanol (MeOH) and dimethyl ether (DME) selectivity excluding CO were calculated with the followed equations.

$$CO_2 \text{ conversion} = (CO_{2in} - CO_{2out})/(CO_{2in}) \times 100\% \quad (1)$$

CO_{2in}: moles of CO_2 at the inlet;
CO_{2out}: moles of CO_2 at the outlet;

$$CO \text{ selectivity} = CO_{out}/(CO_{2in} - CO_{2out}) \times 100\% \quad (2)$$

CO_{out}: moles of CO at the outlet;

$$C_nH_m \text{ selectivity} = N_{CnHm}/(\text{All the carbon atoms of products in FID}) \times 100\% \quad (3)$$

MeOH selectivity = N_{MeOH}/(All the carbon atoms of products in FID) × 100%.
DME selectivity = N_{DME}/(All the carbon atoms of products in FID) × 100%.
N_{CnHm}: the number of carbon atoms for C_nH_m;
N_{MeOH}: the number of carbon atoms for MeOH;
N_{DME}: the number of carbon atoms for DME.

2.3. Catalyst characterization

The XRD tests were performed on a PANalytical X'Pert PRO X-ray diffractometer (XRD) with Cu Kα radiation. Element analysis was carried out on a Philips Magix-601 X-ray fluorescence (XRF) spectrometer. Nitrogen adsorption–desorption isotherms at 77 K were obtained on a Micromeritics ASAP 2020, the BET model was used to estimate the surface areas of all the samples. The solid state ^1H MAS NMR experiments were conducted on Bruker AvanceIII spectrometer equipped with 9.4 T magnet, ^1H MAS NMR spectra were recorded using one pulse sequence with spinning rate of 12 kHz. 32 scans were accumulated with recycle delay 10 s. SEM measurements were performed on an SU8020 scanning electron microscopy. The nanostructure of the catalysts was investigated by using a Tecnai G2F20 (200 kV) high-resolution transmission electron microscope (TEM) (FEI, Holland) equipped with a X-ray microprobe of 0.14 nm optimum resolution for energy dispersive X-ray spectroscopy (EDS) and the instrument can reach a maximum resolution of 0.15 nm/200 kV. X-ray photoelectron spectroscopy (XPS) measurements were performed on a Thermofisher ESCALAB 250Xi spectrometer. H_2-temperature programmed reduction (H_2-TPR) and NH_3-temperatrue programmed desorption (NH_3-TPD) and CO_2-temperature-programmed desorption (CO_2-TPD) of analysis of samples (before test, all the samples were reduced at 573 K for 4 h with 20 mL/min H_2) were investigated by 2910 Automatic chemical adsorption instrument (Micromeritics, United States) from room temperature to 973 K with a ramp of 10 K/min. *In-situ* DRIFTS studies were performed on a Bruker Tensor 27 instrument with a MCT detector. $InZrO_x$ powder was pressed into a diffuse reflectance infrared cell with ZnSe window. First, $InZrO_x$ was treated by 25 mL min^{-1} H_2/Ar (H_2/Ar = 3/7) mixture at 0.1 MPa and 323 K for 0.5 h and the background spectrum was recorded. Then, 25 mL min^{-1} mixed gas (H_2/CO_2 = 3/1) was introduced and the *in-situ* DRIFT spectra obtained by collecting 32 scans at 4 cm^{-1} resolution were recorded under the same conditions. The organic materials retained in SSZ-13 after reactions were analyzed by M. Guisnet's method. Spent SSZ-13 catalyst were dissolved in HF solution (20 wt%). After being neutralized with sodium hydroxide solution (5 wt%), the soluble organics were extracted by CH_2Cl_2 (containing 10 ppm C_2Cl_6) and then analyzed by using a GC–MS instrument (Agilent 7890B) equipped with an HP-5 capillary column.

3. Results and discussion

Hydrogenation of CO_2 over $InZrO_x$ + SSZ-13 composite catalyst with weight ratio of 2:1 has been performed at 623 K, H_2/CO_2 = 3/1 and 4.0 MPa. As shown in Fig. 1(a), the propane is primary product in the hydrocarbon products kept at ~70% with ~24% CO_2 conversion and ~61% CO selectivity during 100 h test. Furthermore, the LPG in hydrocarbons reaches up to ~90%, which is much higher

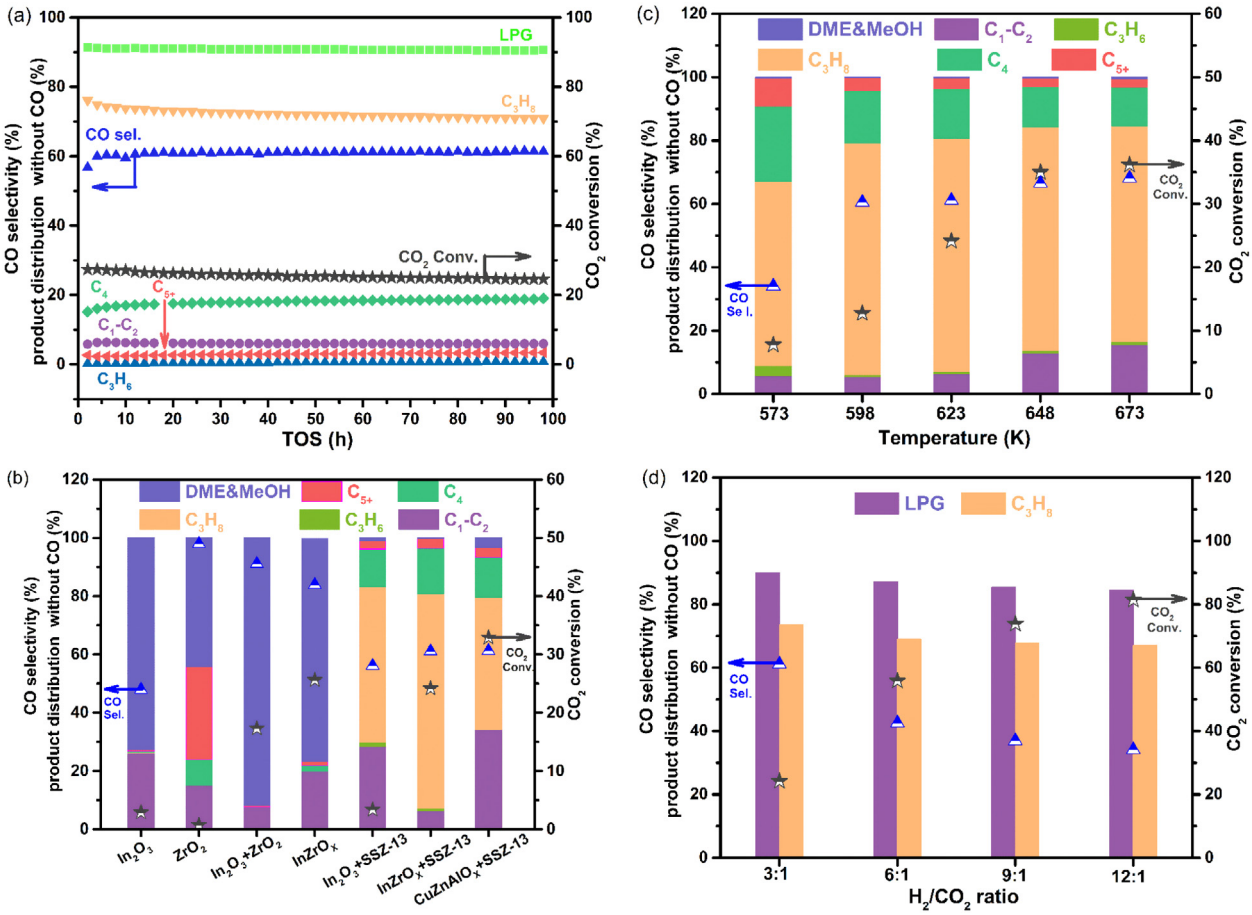

Fig. 1. Catalytic results for CO_2 hydrogenation. (a) CO_2 hydrogenation over $InZrO_x$ + SSZ-13. Catalyst weight = 600 mg, weight ratio of OX/ZEO = 2, GHSV = 1000 mL·g^{-1}·h^{-1}, 4.0 MPa, 623 K, $H_2/CO_2/Ar$ = 3/1/0.2. (b) Comparisons of catalytic performance over various catalysts. Catalyst weight = 300 mg, weight ratio of OX/ZEO = 2, GHSV = 1000 mL·g^{-1}·h^{-1}, 4.0 MPa, 623 K, $H_2/CO_2/Ar$ = 3/1/0.2. (c) The effect of reaction temperature for $InZrO_x$ + SSZ-13. Catalyst weight = 300 mg, weight ratio of OX/ZEO = 2, GHSV = 1000 mL·g^{-1}·h^{-1}, 4.0 MPa, $H_2/CO_2/Ar$ = 3/1/0.2. (d) The effect of H_2/CO_2 ratio for $InZrO_x$ + SSZ-13. Catalyst weight = 300 mg, weight ratio of OX/ZEO = 2, GHSV = 1000 mL·g^{-1}·h^{-1}, 4.0 MPa, 623 K.

than those over Cu-Zn-Al@H-Beta and InO_x/H-ZSM-5 in the previous works [36–39], the total CH_4, C_2H_6 and C_2H_4 in the hydrocarbons is less than 6%. As shown in Fig. 1(b), the pure InO_x oxide shows only 4.3% CO_2 conversion with 72.4% methanol in the product and only 25% CO selectivity, meanwhile the monoclinic ZrO_2 (m-ZrO_2) is almost inert for CO_2 conversion. Interestingly, compared with pure InO_x or m-ZrO_2, the $InZrO_x$ oxide which was produced by doping In to m-ZrO_2 shows an obvious improved catalytic activity. The conversion of CO_2 reaches up to 26.8% with 74.8% methanol. Results above suggest that In species may be the primary sites to catalyze CO_2 hydrogenation and their structures could be changed after doping on the m-ZrO_2. After mixing the oxides (InO_x or $InZrO_x$) and SSZ-13, the CO_2 conversion does not change significantly, but propane become the main product. It indicates that CO_2 hydrogenation over the composite catalyst such as InO_x + SSZ-13 or $InZrO_x$ + SSZ-13 is a typical tandem process. The performance of $CuZnAlO_x$ oxide mixed with SSZ-13 is also investigated. As expected, higher CO_2 conversion was obtained, whereas selectivity of propane was only 45.3% with 27.2% ethane and 13.7% butane in hydrocarbons, which is possibly attributed to strong ability of hydrogenation within Cu-based catalyst. It is clear that conventional methanol synthesis catalysts such as $CuZnAlO_x$ oxide are not suitable for the CO_2 hydrogenation to propane. Thus, the hydrogenation ability of oxide is important to obtain a high selectivity of propane. The catalytic behaviors for these composite catalysts demonstrate that SSZ-13 is the main factor for the selective formation of propane, but oxides also affect it. As the reaction temperature increased from 573 to 673 K, the conversion of CO_2 improves by about 2 times, but the selectivity of propane in hydrocarbons

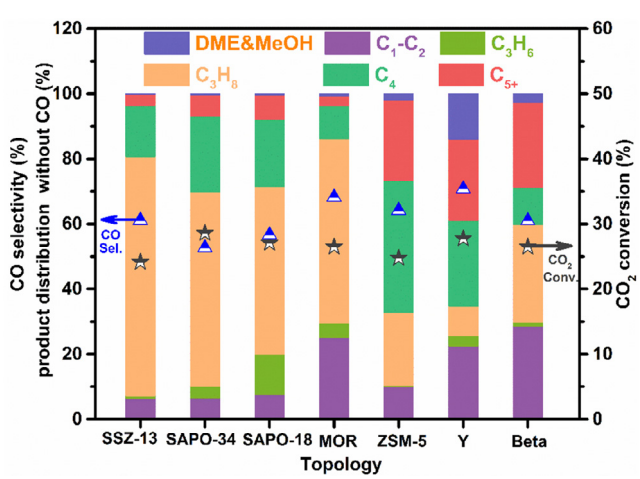

Fig. 2. Effect of molecular sieve topology in the composite catalyst on the performance of CO_2 hydrogenation. Catalyst weight = 300 mg, weight ratio of OX/ZEO = 2, GHSV = 1000 mL·g^{-1}·h^{-1}, 4.0 MPa, 623 K, $H_2/CO_2/Ar$ = 3/1/0.2. The oxide in the composite catalysts is $InZrO_x$.

is less affected (Fig. 1c). As the H_2/CO_2 molar ratio increases from 3 to 12, the CO_2 conversion is essentially increased from 20% to 80%, while the CO selectivity is obviously decreased from 60% to 35%. The propane or LPG in hydrocarbons is almost unchanged. That is to say, increasing the proportion of hydrogen is a good way to suppress the reverse water gas shift reaction (RWGS). This may be valuable for industrialization because hydrogen is relatively easy to separate. Moreover, as shown in Fig. S1, increasing contact time benefits the CO_2 conversion and propane selectivity.

Considering that the selectivity of propane in CO_2 hydrogenation could be mainly related to the topology of the molecular sieves in composite catalysts, the performances of $InZrO_x$ oxides mixed with a series of molecular sieves are explored (Fig. 2). It can be observed that H-Y, H-ZSM-5, and H-Beta are easy to generate hydrocarbons with more than 3 carbon atoms. It suggests that 10 and 12 MR micropores could be beneficial to form hydrocarbons with larger size than propane. It can be noted that the propane selectivity over bifunctional catalyst containing H-MOR with 8 and 12 MR micropores is much higher than those three zeolites above. It is possible that 8 MR micropores play a more important role than 12 MR micropores in the selective generation of propane. In addition, the propane selectivity over bifunctional catalysts containing SAPO molecular sieve (SAPO-34 or SAPO-18) with only 8 MR micropores is approximate to that containing H-MOR. It further indicates that the 8 MR micropores facilitate propane generation, which may be due to their similar sizes. It can be found that compared with SAPO-34, SSZ-13 molecular sieve is more conductive to propane generation, even though they have the same topological structure. The acid properties of these two molecular sieves generally vary widely, which may have an effect on propane selectivity.

Composite catalysts containing $InZrO_x$ oxide and SSZ-13 zeolites with various Brønsted acid density are compared in the CO_2 hydrogenation reaction. These SSZ-13 zeolites were prepared with different concentrations of NH_4NO_3 aqueous solution twice. The density of strong and Brønsted acid sites were calculated by NH_3-TPD and ^1H MAS NMR analysis, respectively, as shown in Fig. S2(a and b) and the results as listed in Table S4. It is clear from Fig. 3(a) that as the Brønsted acid density increases, the propane selectivity is obviously improved at the expense of MeOH and C_{2-4} olefins. It suggests that the propane may come from the tandem reactions of MTO and olefin hydrogenation, both of which are catalyzed by the Brønsted acids. Notably, the Brønsted acid density of SAPO-34 is higher than SSZ-13 (Fig. S2(c), Table S4), while the former produces lower propane selectivity (Fig. 2). It can be found from the results of NH_3-TPD analysis in Fig. 3(b) that the acid strengthen for SSZ-13 is much higher than SAPO-34. It means that not only the density of the Brønsted acid but also the strength of the acid plays an important role in the formation of propane.

3.1. Structural characterization

XRD patterns (Fig. 4a) show that the InO_x or ZrO_2 have typical cubic or monoclinic crystal phase (JCPDS NO. 06-0416 and JCPDS NO. 37-1484), respectively. The crystal phase of $InZrO_x$ is their combination. By using the Scherrer equation to calculate the peaks at 21.5° and 35.5° (Table S1), which are assigned to (2 1 1), (4 0 0) planes of InO_x, it can be found that the size of InO_x particles (14 nm) supported on the monoclinic ZrO_2 is smaller than the pure InO_x (20 nm). The XRD patterns for Na-SSZ-13 and SAPO-34 in Fig. S3 indicate that they all have a CHA topology. As listed in Table S2, the BET surface area of $InZrO_x$ (24.6 m^2/g) is much higher than InO_x (6.5 m^2/g) or m-ZrO_2 (4.9 m^2/g), which is mainly due to the smaller size of the loaded InO_x particles. The SEM image of SSZ-13 (Fig. S4) suggests that its crystal size is ~50 nm. By comparing the SEM images of $InZrO_x$ and m-ZrO_2 (Fig. S4), it is apparent that the InO_x small particles are supported on the ZrO_2 carrier for $InZrO_x$ sample. The high-resolution transmission electronic microscopy (HRTEM) image of $InZrO_x$ sample is exhibited in Fig. 4(b). The fringe spacing of 0.32 and 0.28 nm could be corresponded to (−1 1 1) and (1 1 1) planes of ZrO_2 crystals. Meanwhile the fringe spacing of 0.30 and 0.42 nm could be assigned to (−1 1 1) and (1 1 1) planes of InO_x crystals. The element distribution analysis (Fig. S5) demonstrates that the InO_x are highly dispersed on ZrO_2 carrier. As presented in Fig. 4(c), two distinct peaks can be divided from the O 1s XPS spectra of $InZrO_x$ and InO_x oxides. One peak located at a higher binding energy of 531.6 eV is generally considered as the oxygen atoms adjacent to an oxygen vacancy ($O_{vacancy}$), meanwhile the other peak at a lower binding energy of 529.6 eV is assigned to the lattice oxygen atoms ($O_{lattice}$) [40,41]. Basing on the deconvolution results of O 1*s* XPS signal (Table S3), the amount of defect oxygen for $InZrO_x$ is much higher than InO_x. The oxygen vacancies are generally acted as sites to activate CO_2, which could result in that the catalytic activity of $InZrO_x$ is much higher than InO_x (Fig. 1b).

It can be observed from the H_2-TPR results (Fig. 5a) that m-ZrO_2 is very stable and cannot be reduced by H_2 within the range of reaction temperature, For the bulk InO_x the reduction peak of InO_x oxide is centered at about 515 K, which is approximate to the findings in the previous literatures [42,43]. Interestingly, compared with InO_x, $InZrO_x$ exhibits a lower temperature peak centered at 458 K, indicating that the InO_x species supported on m-ZrO_2 are easier to reduce. Smaller and more dispersed InO_x particles for

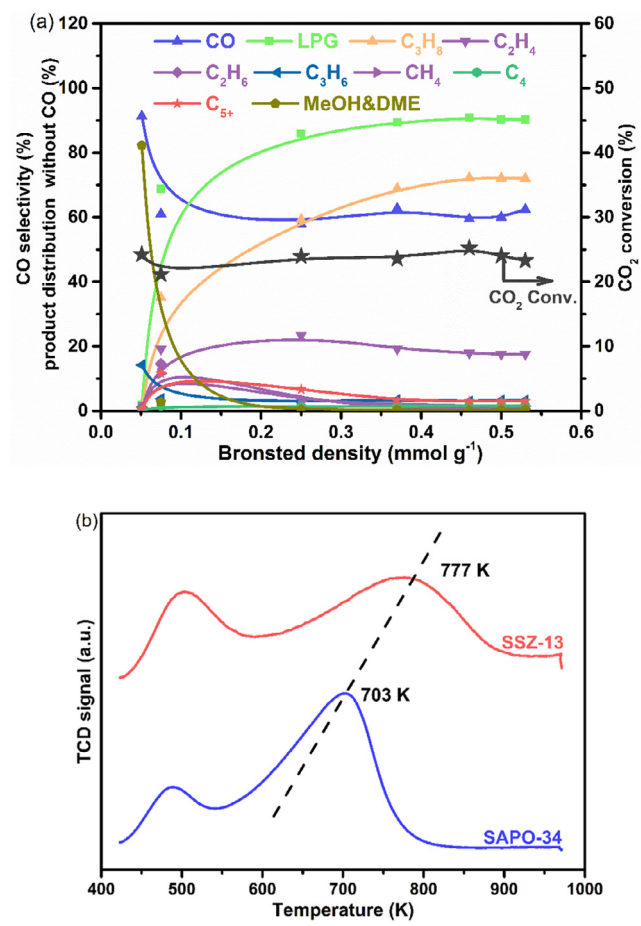

Fig. 3. The effect of acid property for SSZ-13 on catalytic performances of the composite catalysts. (a) The effect of acid density of SSZ-13. Catalyst weight = 300 mg, GHSV = 1000 mL·g^{-1}·h^{-1}, 4.0 MPa, 623 K, $H_2/CO_2/Ar$ = 3/1/0.2. The oxides in the composite catalysts are $InZrO_x$. (b) NH_3-TPD profiles of SSZ-13 and SAPO-34 zeolites.

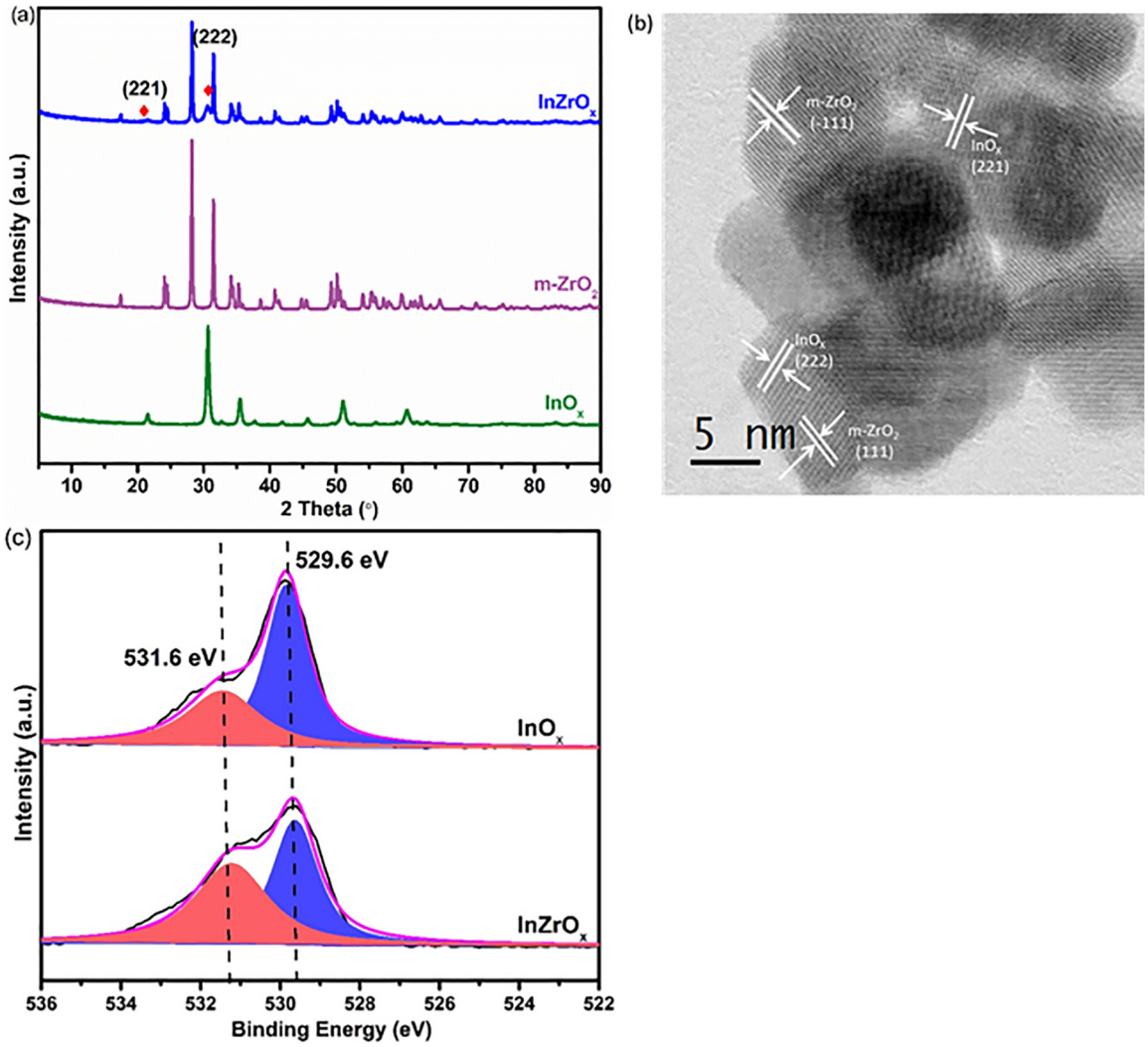

Fig. 4. Structural characteristics of In-based oxides. (a) XRD patterns of InO_x, monoclinic ZrO_2 and $InZrO_x$ oxides. (b) HRTEM image of $InZrO_x$, (c) O 1*s* XPS spectra of InO_x and $InZrO_x$ oxides.

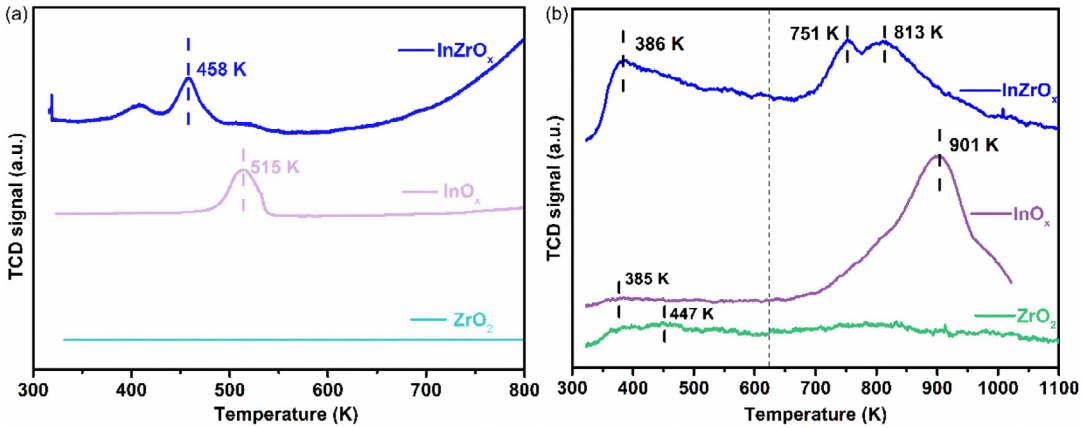

Fig. 5. Results of the reduction and adsorption ability tests for the oxides. (a) H_2-TPR results, (b) CO_2-TPD results for the reduced oxides.

$InZrO_x$ may be more conducive to reduction. Fig. 5(b) shows the CO_2-TPD results of InO_x, ZrO_2 and $InZrO_x$ catalysts. As shown in Fig. 5(b), CO_2-TPD results indicate that the m-ZrO_2 has almost no ability to adsorb CO_2. The adsorption of CO_2 on InO_x oxide is so strong that it begins to desorb above 673 K, which is even higher than the suitable temperatures for hydrogenation reaction. Also a weak desorption peak at 385 K for InO_x oxide can be observed, which is in accordance with the previous work [26]. Different from

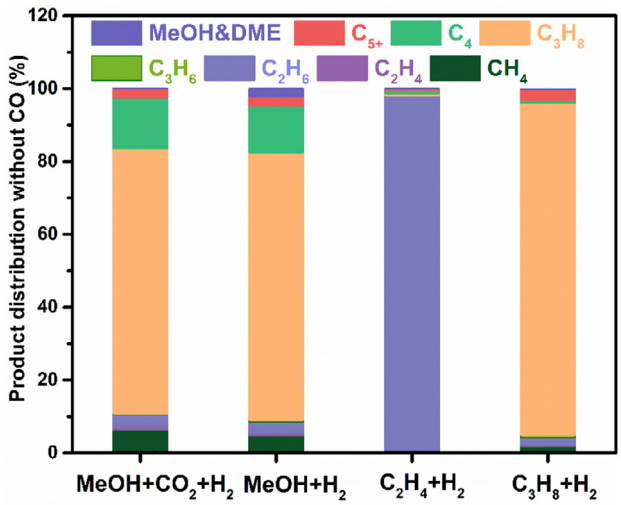

Fig. 6. Products distribution of methanol and olefins conversion with CO_2 + H_2 or H_2 co-feed over SSZ-13 zeolite. Reaction conditions: 4.0 MPa, 623 K.

the two oxides, $InZrO_x$ not only has better CO_2 adsorption performance, but also partly desorbs below 673 K. In general, the moderate binding capacity of the heterogeneous catalyst to the reaction molecules is beneficial to the catalytic cycle. This could explain that the CO_2 hydrogenation performance of $InZrO_x$ is higher than the other two catalysts.

The in-situ DRIFTS of CO_2 hydrogenation over $InZrO_x$ at 0.1 MPa are explored. It is obvious from Fig. S6 that absorbed surface formate species (1620, 1375 and 2910 cm^{-1}) were firstly generated, then, absorbed surface methoxy species (2940 and 2840 cm^{-1}) were formed by hydrogenation of formate species. The soluble carbonaceous deposits in SSZ-13 zeolite of bifunctional catalyst $InZrO_x$ + SSZ-13 after reaction were analyzed by GC–MS and organic species retained in SSZ-13 component are analogous. As shown in Fig. S7, methylbenzenes (species of 1–5), methylnaphthalenes (species of 7–9) and phenathrene (species of 10–11) are observed. These aromatic species, in particular the methylbenzenes (species of 1–5) were considered as the "hydrocarbon pool" intermediates [44], hence, MTO reaction occurred in CO_2 to propane. Therefore, it was considered that CO_2 hydrogenation to propane reaction over composite catalyst $InZrO_x$ + SSZ-13 is substantially the combination of methanol synthesis and MTO reactions. In addition, propane was the main product in methanol conversion over SSZ-13 with CO_2 + H_2 or H_2 co-feeding also supports that methanol was likely to be an intermediate in CO_2 hydrogenation to propane. Moreover, Fig. 6 shows that SSZ-13 can catalyze olefins (including ethylene and propylene) hydrogenation to paraffins. Therefore, combined with all above the catalytic results, it is clearly demonstrated that propane is produced through CO_2 hydrogenation over bifuncitonal catalyst $InZrO_x$ + SSZ-13 as follows: firstly, the surface formate species are firstly formed and then hydrogenated to surface methoxy species on $InZrO_x$; MeOH generated from the dissociation of methoxy species is transmitted to SZZ-13 to primarily propylene by dual cycle mechanism [45–50], finally, propylene hydrogenation to propane consecutively take place over SSZ-13.

4. Conclusions

In summary, highly selective conversion of CO_2 hydrogenation to propane has been firstly achieved over a composite catalyst $InZrO_x$ + SSZ-13. The propane selectivity reaches up to 75% at 623 K and no obvious deactivation is observed in 100 h test. Combined the catalytic results with FT-IR characterization, $InZrO_x$ is responsible for the hydrogenation of CO_2 to methanol, while the topology of zeolite and acidity of SSZ-13 account for C–C coupling reaction in tadem. The 8-MR micropores and the higher strength of the acid within SSZ-13 benefit the formation of propane. Compared with pure InO_x and ZrO_2, the composite oxide $InZrO_x$ contains more oxygen vacancies, is more readily reduced by H_2, and is easier to adsorb and desorb CO_2 within the reaction temperature, which benefits the activation and conversion of H_2 and CO_2. Furthermore, this work demonstrates that composite catalyst $InZrO_x$ + SSZ-13 showed excellent stability over 100 h on stream without obvious deactivation, which suggested its potential application in manufacturing propane from CO_2 hydrogenation.

Declaration of Competing Interest

The authors declare that they have no known competing financial interests or personal relationships that could have appeared to influence the work reported in this paper.

Acknowledgments

We acknowledge the financial support from the National Natural Science Foundation of China (Grant Nos. 21978285, 21991093, 21991090), and the "Transformational Technologies for Clean Energy and Demonstration", Strategic Priority Research Program of the Chinese Academy of Sciences (Grant No. XDA21030100).

Appendix A. Supplementary data

Supplementary data to this article can be found online at https://doi.org/10.1016/j.jechem.2020.04.069.

References

[1] H. Rao, L.C. Schmidt, J. Bonin, M. Robert, Nature 548 (2017) 74–77.
[2] B. An, Z. Li, Y. Song, J.Z. Zhang, L.Z. Zeng, C. Wang, W.B. Lin, Nat. Catal. 2 (2019) 709–717.
[3] S.X. Ren, D. Joulié, D. Salvatore, K. Torbensen, M. Wang, M. Robert, C.P. Berlinguette, Science 365 (2019) 367–369.
[4] W. Zhou, K. Cheng, J.C. Kang, C. Zhou, V. Subramanian, Q.H. Zhang, Y. Wang, Chem. Soc. Rev. 48 (2019) 3193–3228.
[5] F.S. Karn, J.F. Shultz, R.B. Anderson, Ind. Eng. Chem. Prod. Res. Devel. 4 (1965) 265–269.
[6] E. Moioli, R. Mutschler, A. Züttel, Renewable Sustainable Energy Rev. 107 (2019) 497–506.
[7] Q.P. Cheng, Y. Tian, S.S. Lyu, N. Zhao, K. Ma, T. Ding, Z. Jiang, L.H. Wang, J. Zhang, L.R. Zheng, F. Gao, L. Dong, N. Tsubaki, X. Li, Nat. Commun. 9 (2018) 3250–3258.
[8] V.P. Santos, T.A. Wezendonk, J.J. Jaen, A.I. Dugulan, M.A. Nasalevich, H.U. Islam, A. Chojecki, S. Sartipi, X. Sun, A.A. Hakeem, A.C. Koeken, M. Ruitenbeek, T. Davidian, G.R. Meima, G. Sankar, F. Kapteijn, M. Makkee, J. Gascon, Nat. Commun. 6 (2015) 6451–6458.
[9] L.S. Zhong, F. Yu, Y.L. An, Y.H. Zhao, Y.H. Sun, Z.J. Li, T.J. Lin, Y. Lin, X. Qi, Y. Dai, L. Gu, J. Hu, S. Jin, Q. Shen, H. Wang, Nature 538 (2016) 84–87.
[10] G.L. Bezemer, J.H. Bitter, H.P.C.E. Kuipers, H. Oosterbeek, J.E. Holewijn, X.D. Xu, F. Kapteijn, A.J.V. Dillen, K.P.D. Jong, J. Am. Chem. Soc. 128 (2006) 3956–3964.
[11] R.B. Anderson, J. Catal. 55 (1978) 114–115.
[12] F. Jiao, J.J. Li, X.L. Pan, J.P. Xiao, H.B. Li, H. Ma, M.M. Wei, Y. Pan, Z.Y. Zhou, M.R. Li, M. Shu, J. Li, Y.F. Zhu, D. Xiao, T. He, J.H. Yang, F. Qi, Q. Fu, X.H. Bao, Science 351 (2016) 1065–1068.
[13] K. Cheng, B. Gu, X.L. Liu, J.C. Kang, Q.H. Zhang, Y. Wang, Angew. Chem. Int. Ed. 128 (2016) 4803–4806.
[14] F. Jiao, X.L. Pan, K. Gong, Y.X. Chen, G. Li, X.H. Bao, Angew. Chem. Int. Ed. 57 (2018) 4692–4696.
[15] N. Li, F. Jiao, X.L. Pan, Y.X. Chen, J.Y. Feng, G. Li, X.H. Bao, Angew. Chem. Int. Ed. 58 (2019) 7400–7404.
[16] Y.F. Zhu, X.L. Pan, F. Jiao, J. Li, J.H. Yang, M.Z. Ding, Y. Han, Z. Liu, X.H. Bao, ACS Catal. 7 (2017) 2800–2804.
[17] J.H. Yang, X.L. Pan, F. Jiao, J. Li, X.H. Bao, Chem. Commun. 53 (2017) 1146–1149.
[18] N. Li, F. Jiao, X.L. Pan, Y. Ding, X.H. Bao, ACS Catal. 9 (2019) 960–996.
[19] W. Zhou, S.L. Shi, Y. Wang, L. Zhang, Y. Wang, G.Q. Zhang, X.J. Min, K. Cheng, Q. H. Zhang, J.C. Kang, Y. Wang, ChemCatChem 11 (2019) 1681–1688.
[20] X.L. Liu, W. Zhou, Y.D. Yang, K. Cheng, J.C. Kang, L. Zhang, G.Q. Zhang, X.J. Min, Q.H. Zhang, Y. Wang, Chem. Sci. 9 (2018) 4708–4718.

[21] K. Cheng, J.C. Kang, Q.H. Zhang, Y. Wang, Sci. China Chem. 11 (2017) 12–15.
[22] C. Kang, J. Kang, S. Huang, Z. You, W. Ye, ACS Catal. 2 (2012) 441–449.
[23] W. Zhou, J.C. Kang, K. Cheng, S. He, J.Q. Shi, C. Zhou, Q.H. Zhang, J.C. Chen, L.M. Peng, M.S. Chen, Y. Wang, Angew. Chem. Int. Ed. 57 (2018) (2016) 12012–12021.
[24] Z.L. Li, J.J. Wang, Y.Z. Qu, H.L. Liu, C.Z. Tang, S. Miao, Z.C. Feng, H.Y. An, C. Li, ACS Catal. 7 (2017) 8544–8548.
[25] X.L. Liu, M.H. Wang, C. Zhou, W. Zhou, K. Cheng, J.C. Kang, Q.H. Zhang, W.P. Deng, Y. Wang, Chem. Commun. 54 (2017) 140–143.
[26] P. Gao, S.S. Dang, S.G. Li, O.X. Bu, Z.Y. Liu, M.H. Qiu, C.G. Yang, H. Wang, L.S. Zhong, Y. Han, Q. Liu, W. Wei, Y.H. Sun, A.C.S. Catal, ACS Catal. 8 (2018) 571–578.
[27] Z. Bo, P. Zhai, P.F. Wang, J.Q. Li, T. Li, M. Peng, M. Zhao, G. Hu, Y. Yang, Y. Wang, Q.W. Zhang, W.B. Fan, D. Ma, Chem 3 (2017) 323–333.
[28] K. Cheng, W. Zhou, J.C. Kang, S. He, S.L. Shi, Q.H. Zhang, Y. Pan, W. Wen, Y. Wang, Chem 3 (2017) 334–347.
[29] Z.L. Li, Y.Z. Qu, J.J. Wang, H.L. Liu, M.R. Li, S. Miao, C. Li, Joule 3 (2019) 570–583.
[30] Y.M. Ni, Z.Y. Chen, Y. Fu, Y. Liu, W.L. Zhu, Z.M. Liu, Nat. Commun. 9 (2018) 3457–3463.
[31] Y.F. Xu, J.G. Liu, J. Wang, G.G. Ma, J.H. Lin, Y. Yang, Y.W. Li, C.H. Zhang, M.Y. Ding, ACS Catal. 9 (2019) 5147–5156.
[32] J.H. Yang, K. Gong, D.Y. Miao, F. Jiao, X.L. Pan, X.J. Meng, F.S. Xiao, X.H. Bao, J. Energy Chem. 35 (2019) 44–48.
[33] P. Gao, S.G. Li, X.N. Bu, S.S. Dang, Z.Y. Liu, H. Wang, L.S. Zhong, M.H. Qiu, C.G. Yang, J. Cai, W. Wei, Y.H. Sun, Nat. Chem. 9 (2017) 1019–1024.
[34] W.H. Li, H.Z. Wang, X. Jiang, J. Zhu, Z.M. Liu, X.W. Guo, C.S. Song, RSC Adv. 8 (2018) 7651–7669.
[35] M.T. Arslan, B.A. Qureshi, S.Z.A. Gilani, D. Cai, Y.H. Ma, M. Usman, X. Chen, Y. Wang, F. Wei, ACS Catal. 9 (2019) 2203–2212.
[36] P. Lu, J. Sun, D.M. Shen, R.Q. Yang, C. Xing, C.X. Lu, N. Tsubaki, S.T. Shan, Appl. Energy 209 (2018) 1–7.
[37] L. Peng, D.M. Shen, S.L. Cheng, E. Hondo, L.G. Chizema, C.W. Wang, X.K. Gai, C.X. Lu, R.Q. Yang, Fuel 223 (2018) 157–163.
[38] X.G. Ma, Q.J. Ge, J.G. Ma, H.Y. Xu, Fuel Process. Technol. 109 (2013) 1–6.
[39] C. Kang, B. Gu, X.L. Liu, J.C. Kang, Q.H. Zhang, Y. Wang, Angew. Chem. Int. Ed. 128 (2016) 4803–4806.
[40] Z.P. Liu, Y. Xu, J.M. Cheng, W.H. Wang, B.W. Wang, Z.H. Li, X.B. Ma, Appl. Surf. Sci. 433 (2018) 730–738.
[41] D.W. Jeong, H.S. Na, J.O. Shim, W.J. Jang, H.S. Roh, Catal. Sci. Technol 5 (2015) 3706–3713.
[42] O. Martin, A.J. Martín, C. Mondelli, S. Mitchell, T.F. Segawa, R. Hauert, C. Drouilly, D. Curulla-Ferré, J. Pérez-Ramírez, Angew. Chem. Int. Ed. 55 (2016) 6261–6265.
[43] S.S. Dang, P. Gao, Z.Y. Liu, X.Q. Chen, C.G. Yang, H. Wang, L.S. Zhong, S.G. Li, Y.H. Sun, J. Catal. 364 (2018) 382–393.
[44] Y.M. Ni, Y. Liu, Z.Y. Chen, M. Yang, H.C. Liu, Y.L. He, Y. Fu, W.L. Zhu, Z.M. Liu, ACS Catal. 9 (2018) 1026–1032.
[45] S. Svelle, U. Olsbye, F. Joensen, M. Bjorgen, J. Phys. Chem. C 111 (2007) 17981–17984.
[46] J.R. Chen, J.Z. Li, C.Y. Yuan, S.T. Xu, Y.X. Wei, Q.Y. Wang, Y. Zhou, J.B. Wang, M.Z. Zhang, Y.L. He, Z.M. Liu, Catal. Sci. Technol. 4 (2014) 3268–3277.
[47] Z.Q. Liu, Y.Y. Chu, X.M. Tang, L. Huang, G.C. Li, X.F. Yi, A.M. Zheng, J. Phys. Chem. C 121 (2017) 22872–22882.
[48] S. Svelle, S. Kolboe, O. Swang, U. Olsbye, J. Phys. Chem. B 109 (2005) 12874–12878.
[49] A. Hwang, M. Kumar, J.D. Rimer, A. Bhan, J. Catal. 346 (2017) 154–160.
[50] I. Yarulina, A.D. Chowdhury, F. Meirer, B.M. Weckhuysen, J. Gascon, Nat. Catal. 1 (2018) 398–411.